ISSN: 2472-3703 DOI: 10.6911/WSRJ.202602_12(2).0005

Flow Characteristics and Cavitation Behavior of an Industrial Gate Valve Based on CFD and Fluid–Structure Interaction Analysis

Chengjun Zhang [1, *], Xiaomin Yang [2]

[1]Qiqihar University, Qiqihar 161006, Heilongjiang, China

[2]Zhengbai Valve Co., Ltd., Wenzhou 325000, Zhejiang, China

[*] Corresponding author

Abstract

To reduce the dependence of small- and medium-sized enterprises on physical experiments during valve research and development, this study employs the SolidWorks Flow Simulation module to visualize and analyze the internal flow field of a DN100 industrial gate valve under different opening conditions. A steady-state computational fluid dynamics (CFD) model is established to systematically investigate the flow characteristics, pressure drop, flow resistance coefficient, and cavitation-sensitive regions at various valve openings. The influence of valve opening reduction on internal flow behavior and cavitation evolution is revealed. The results indicate that, with decreasing valve opening, the internal flow field exhibits pronounced pressure drops, significant velocity variations, and an expansion of cavitation-sensitive regions. At small openings, a distinct negative-pressure zone forms on the leeward side of the gate plate, accompanied by strong vortical structures and high-velocity jet flows. Meanwhile, the cavitation region expands progressively as the opening decreases, indicating an increased cavitation risk. The present study provides a valuable theoretical reference for analyzing valve flow characteristics under complex operating conditions.

Keywords

Gate valve; Computational fluid dynamics; Cavitation; Flow characteristics; Structural optimization.

1. INTRODUCTION

Valves are critical components in process industries and energy equipment, directly affecting system safety, operational stability, and energy efficiency. Under high-parameter and complex operating conditions, prototype testing alone is often insufficient to reveal the coupled mechanisms of three-dimensional internal flow, cavitation, pressure pulsation, and structural response during the early stages of valve development. This limitation results in long iteration cycles, high costs, and increased technical risks. With the rapid development of computational fluid dynamics (CFD), multiphysics coupling techniques, and high-performance computing, numerical simulation has become an indispensable tool for valve design and optimization. CFD-based virtual prototyping enables parametric investigations over multiple openings and operating conditions, providing key performance indicators such as pressure drop, flow and resistance coefficients, cavitation-prone regions, flow-induced vibration, and stress concentration zones. These insights offer quantitative guidance for lightweight design and reliability enhancement [1].

ISSN: 2472-3703 DOI: 10.6911/WSRJ.202602_12(2).0005

Previous studies have established multi-level research paradigms ranging from local valve flow analysis to system-level simulations. For ultra-supercritical safety valves, a closed-loop approach integrating theoretical analysis, CFD, and experiments has been used to identify supersonic regions at the outlet and validate pressure-bearing component strength [2]. In long-distance water conveyance systems, multi-condition CFD simulations based on Fluent have been applied to evaluate flow capacity and energy dissipation efficiency [3]. Investigations on cryogenic butterfly valves revealed that small openings intensify internal vortices and flow non-uniformity, highlighting downstream disturbances induced by throttling [4]. One-dimensional transient models, such as PIPENET and AFT Impulse, demonstrated that valve closing laws at pump outlets play a decisive role in water hammer peaks and protection strategies [5]. For check valves, flow passage optimization combined with CFD significantly reduced flow resistance under fully open conditions [6], while fluid-structure interaction (FSI) analyses identified high-stress and large-displacement regions in valve discs and bodies, enabling improvements in opening/closing performance and drag reduction [7].

Overall, valve numerical simulation is evolving from single-valve modeling toward integrated analysis of devices, piping networks, and control systems. Steady-state Reynolds-averaged Navier-Stokes (RANS) simulations support rapid screening across multiple openings, while transient simulations are introduced when necessary to capture opening/closing processes and water hammer effects. Cavitation and multiphase models, combined with velocity, pressure, and density indicators, are employed to identify negative-pressure zones and cavitation nuclei, guiding anti-cavitation design and material or coating selection. CFD-derived loads are mapped onto structural domains to establish one-way or two-way FSI analyses, closing the loop for stress and displacement evaluation. Coupled with data-driven or intelligent optimization methods, this approach achieves a balance between reliability and lightweight design, ultimately enabling system-level coordination with piping networks and control strategies.

Against this background, the present study focuses on multi-opening internal flow visualization and one-way FSI evaluation of an industrial gate valve. Steady-state RANS simulations are used to characterize throttling-induced high pressure drops, high-velocity jets, and negative-pressure vortices, and to identify cavitation-sensitive regions. Pressure field loads are subsequently mapped to the structural domain to evaluate equivalent stress and displacement. In addition, the influence of geometric parameters, such as fillets and flow passage shapes, on fluid-structure responses and optimization potential is explored, providing a reusable methodological framework for digital prototyping and iterative optimization of industrial gate valves.

2. GEOMETRY AND OPERATING CONDITIONS

2.1. Geometric Model

The computational object is a DN100 industrial gate valve. The geometric model includes the valve body, gate plate, stem, handwheel, and sealing rings in Figure 1. The working medium is water at ambient temperature, with a density of 1000 kg/m^3 and a dynamic viscosity of 0.001 Pa·s. The inlet boundary condition is specified as a uniform velocity of 10 m/s, while the outlet is defined by a static pressure boundary condition. To comprehensively evaluate flow characteristics, ten operating conditions with different valve openings are considered, ranging from fully open to 90% closed, covering flow regimes from large to small flow rates. This multi-opening setup enables systematic analysis of flow field variations under different operating states and reveals the influence of opening on flow characteristics, pressure drop, flow resistance coefficient, and cavitation-sensitive regions. The numerical results provide accurate insights into fluid dynamic behavior under each condition, supporting subsequent structural optimization and design improvements.

ISSN: 2472-3703 DOI: 10.6911/WSRJ.202602_12(2).0005

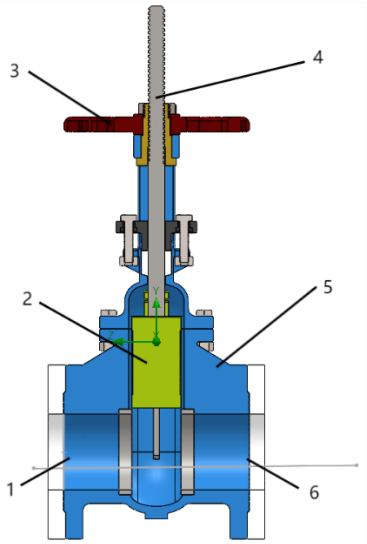


Figure 1. illustrates the valve model, 1. Fluid inlet; 2. Gate plate; 3. Handwheel; 4. Stem; 5. Valve body; 6. Fluid outlet

2.2. Mesh Generation and Independence Verification

A hybrid meshing strategy combining global meshing and local refinement is adopted. Mesh refinement is concentrated in critical regions, including the gap between the gate plate and valve seat, throttling contraction zones, and outlet recirculation regions, to enhance flow resolution and capture small-scale flow features. Mesh independence is verified using three mesh sizes of approximately 280,000, 430,000, and 1.10 million cells. Although the finest mesh provides slightly higher accuracy, it significantly increases computational time. Considering both accuracy and computational efficiency, the mesh with approximately 430,000 cells is selected as the baseline for subsequent analyses in Figure 2. This meshing strategy effectively balances numerical accuracy and resource consumption, ensuring feasible and efficient flow field simulations.

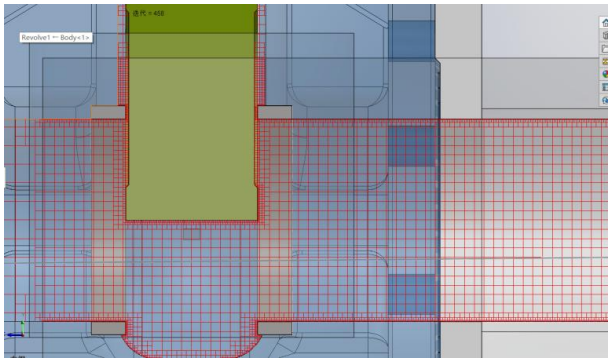


Figure 2. Mesh Division and Locally Refined Areas

2.3. Solver and Physical Models

A steady-state turbulence model is employed to account for turbulent effects in complex flow fields and to simulate nonlinear flow behavior at different valve openings. The turbulence model in Flow Simulation is based on a modified standard k-ε model, enhancing robustness and applicability. The governing equations for turbulent kinetic energy (k) and dissipation rate (ε) are expressed as:

Turbulent kinetic energy (k):

ISSN: 2472-3703 DOI: 10.6911/WSRJ.202602_12(2).0005

$$\frac{\partial(\rho k)}{\partial t}+\frac{\partial(\rho u_j k)}{\partial x_j}=\frac{\partial}{\partial x_j}\left[\left(\mu+\frac{\mu_t}{\sigma_k}\right)\frac{\partial k}{\partial x_j}\right]+P_k-\rho\epsilon$$

Dissipation rate (ε):

$$\frac{\partial(\rho\epsilon)}{\partial t}+\frac{\partial(\rho u_j \epsilon)}{\partial x_j}=\frac{\partial}{\partial x_j}\left[\left(\mu+\frac{\mu_t}{\sigma_\epsilon}\right)\frac{\partial \epsilon}{\partial x_j}\right]+C_{1\epsilon}\frac{\epsilon}{k}P_k-C_{2\epsilon}\rho\frac{\epsilon^2}{k}$$

ρ is the fluid density

u_j denotes the velocity component in the i-th direction.

μ is the molecular (dynamic) viscosity of the fluid.

μ_t is the turbulent viscosity, which is calculated from the turbulent kinetic energy k and the dissipation rate ε.

P_k is the production term of turbulent kinetic energy, $P_k=\mu_t\left(\frac{\partial u_i}{\partial x_j}+\frac{\partial u_j}{\partial x_i}\right)\frac{\partial u_i}{\partial x_j}$ generated by the gradients of the mean velocity field.

$C_{1\epsilon}$, $C_{2\epsilon}$, C_μ, σ_k, σ_ϵ are model constants.

An automatic near-wall treatment is employed. Unlike traditional grid-sensitive wall functions, this approach modifies the formulation of turbulent viscosity, enabling the model to remain applicable in both low-Reynolds-number regions near the wall and high-Reynolds-number regions in the core flow.

The corrected formulation of turbulent viscosity is expressed as:

$$\mu_t=f_\mu\cdot\rho C_\mu\frac{k^2}{\epsilon}$$

The key element of this correction f_μ lies in the damping function, which is defined as a function of the Reynolds number $Re_t=\rho k^2/(\mu\epsilon)$ or a similar characteristic scale. Its role is as follows, in high-Reynolds-number regions ($f_\mu\to1$) away from the wall, the turbulence model asymptotically recovers the standard formulation (k–ε). In low-Reynolds-number regions close to the wall ($f_\mu\to0$), the damping function reduces the turbulent viscosity, thereby allowing the governing equations to be solved directly up to the wall and enabling an explicit resolution of the viscous sublayer. This automated damping function significantly simplifies mesh generation, as there is no strict requirement on the height of the first near-wall cell (y^+); instead, the near-wall physical behavior is adaptively adjusted by the model itself.

To improve model performance under conditions of strong streamline curvature and pronounced pressure gradients, the ε equation is commonly modified. A typical approach introduces a strain-rate-dependent function into the dissipation term, following concepts similar to those adopted in the Realizable *k*–*ε* model or the RNG *k*–*ε* model.

A commonly used generalized form is given as follows:

$$\frac{\partial(\rho\epsilon)}{\partial t}+\ldots=\ldots+C_{1\epsilon}\frac{\epsilon}{k}P_k-C_{2\epsilon}^{*}\rho\frac{\epsilon^2}{k}$$

The modified form of the ε equation can be written as follows:

In this formulation, $C_{2\epsilon}^{*}$ is no longer treated as a constant but as a variable expressed as:

ISSN: 2472-3703 DOI: 10.6911/WSRJ.202602_12(2).0005

$$C_{2\epsilon}^{*}=C_{2\epsilon}+\frac{C_{\mu}\eta^{3}\left(1-\eta/\eta_{0}\right)}{1+\beta\eta^{3}}$$

$\eta=Sk/\epsilon$

$S=\sqrt{2S_{ij}S_{ij}}$ denotes the magnitude of the mean strain rate,

η_0, β is a model constant.

This modification increases the turbulent dissipation rate in regions of rapid strain (large η), thereby yielding predictions that are more consistent with engineering practice.

In addition, the SIMPLE algorithm is employed for pressure-velocity coupling to ensure numerical stability and solution accuracy of the flow field. Cavitation behavior is simulated using the built-in cavitation model of Flow Simulation. This model adopts a transport-equation-based approach similar to the Schnerr-Sauer cavitation model, in which the source terms are derived from a simplified form of the Rayleigh-Plesset equation describing bubble dynamics. The governing expressions are given as follows.

When $p\leq p_{vap}$ (evaporation process, vapor bubble generation):

$$R=C_{dest}\frac{\sqrt{k}}{\sigma}\rho_{l}\rho_{v}\sqrt{\frac{2}{3}\frac{p_{vap}-p}{\rho_{l}}}(1-f_{v})$$

When $p\geq p_{vap}$ (condensation process, bubble collapse):

$$R=-C_{prod}\frac{\sqrt{k}}{\sigma}\rho_{l}\rho_{v}\sqrt{\frac{2}{3}\frac{p-p_{vap}}{\rho_{l}}}f_{v}$$

ρ is the local static pressure,

p_{vap} is the saturation vapor pressure of the liquid (assumed constant at a given temperature),

σ is the surface tension coefficient of the liquid,

k is the local turbulent kinetic energy,

C_{dest} and C_{prod} are empirical constants that control the rates of vapor generation and condensation, respectively.

Based on the inlet turbulence intensity I and the hydraulic diameter DH, the turbulence parameters are calculated using the following relations:

$$I=0.16\left(\frac{\rho_{2}V_{i}D_{H}}{\mu}\right)^{-\frac{1}{8}}$$

$$D_{H}=4\frac{ab}{2(a+b)}$$

The turbulence intensity is set to =2.84%, and the hydraulic diameter is =100 mm.

3. EXPERIMENTAL RESULTS AND ANALYSIS

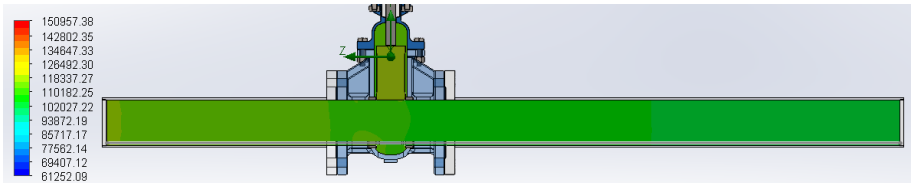
3.1. Pressure Field

Static pressure analysis reveals that pressure drop increases markedly as valve opening decreases, particularly when the opening falls below 30%. At full opening, the flow remains relatively smooth, with a nearly uniform static pressure distribution and minimal pressure loss.

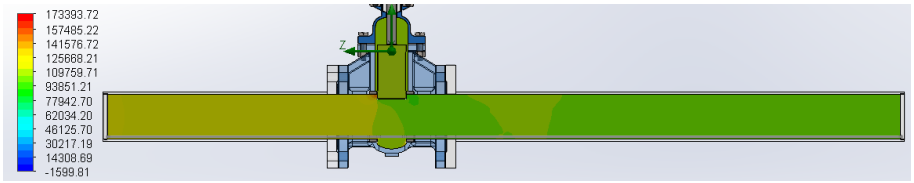
ISSN: 2472-3703 DOI: 10.6911/WSRJ.202602_12(2).0005

As the opening decreases, pronounced pressure non-uniformity emerges. A distinct negative-pressure region forms on the leeward side of the gate plate and expands downstream with decreasing opening, indicating a substantial increase in flow resistance at small openings.

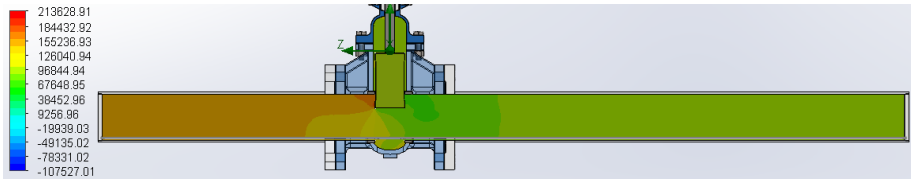
Significant pressure fluctuations are observed in the axial region between 0.55 m and 0.72 m, reflecting the combined effects of geometric contraction and flow acceleration. When the opening is below 50%, static pressure variations exhibit strong nonlinearity, closely associated with accelerated flow and complex fluid dynamics, further intensifying internal flow resistance. These trends are consistent with the static pressure contours shown in Figure 3.



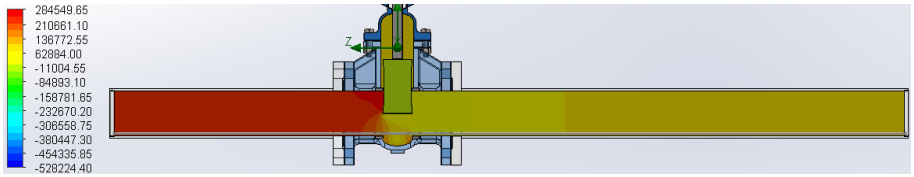
(a) Fully open



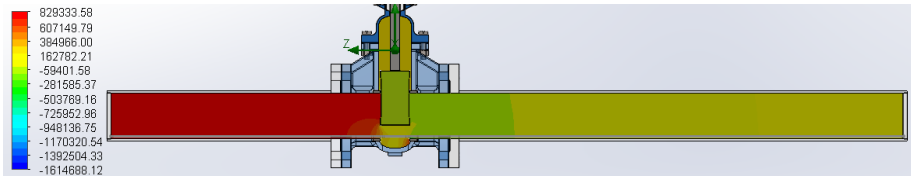
(b) 10% closed



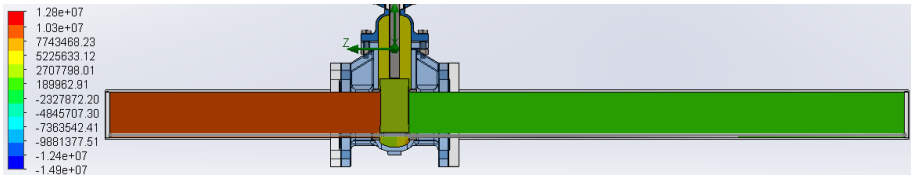
(c) 30% closed



(d) 50% closed



(e) 70% closed



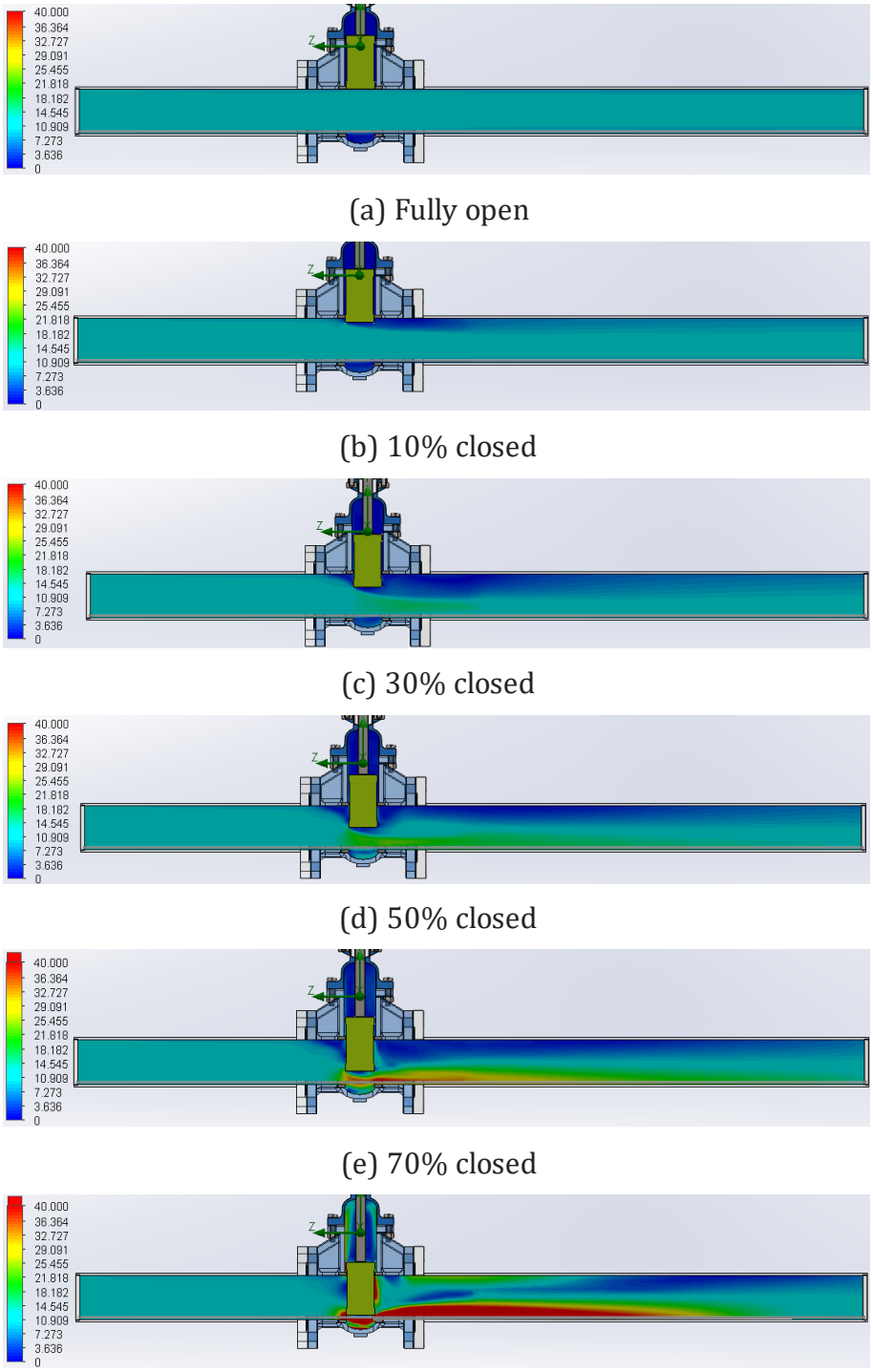
(f) 90% closed

Figure 3. Static pressure contours of the flow field at different valve openings

ISSN: 2472-3703 DOI: 10.6911/WSRJ.202602_12(2).0005

3.2. Velocity Field and Jet Core

With decreasing valve opening, the velocity distribution changes significantly. High-velocity jets form near the lower edge of the gate plate, while a low-velocity expansion layer develops upstream. This behavior represents a typical throttling effect, which becomes particularly pronounced when the opening is below 30%. Velocity peaks occur near inlet and outlet edges and expand upstream as the opening decreases, leading to increased energy losses.



(a) Fully open

(b) 10% closed

(c) 30% closed

(d) 50% closed

(e) 70% closed

(f) 90% closed

Figure 4. Velocity contours of the flow field at different valve openings

Velocity contour plots in Figure 4 corroborate these observations and highlight the intensified flow instability at small openings. Enhanced velocity fluctuations at openings below

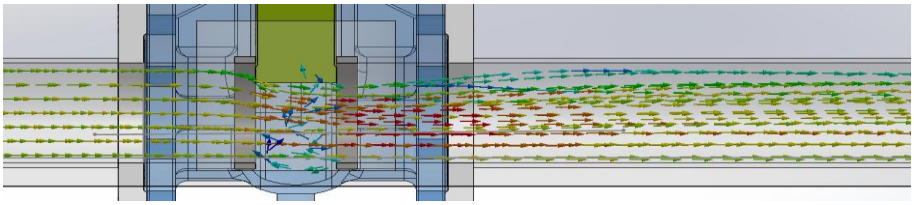
ISSN: 2472-3703 DOI: 10.6911/WSRJ.202602_12(2).0005

30% may trigger complex flow patterns, including strong turbulence and unsteady behavior. Understanding these phenomena is essential for optimizing valve design to reduce energy loss and flow instability.

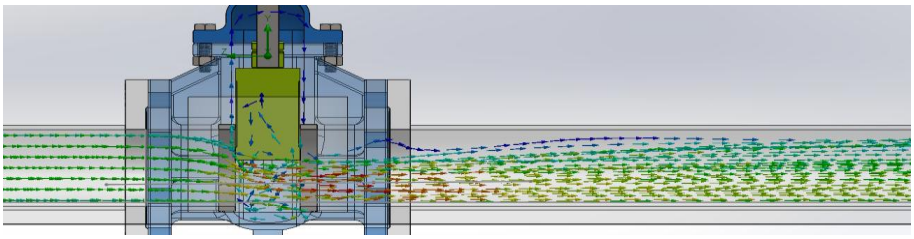
3.3. Streamlines and Recirculation Structures

Streamline analysis provides deeper insight into flow structure evolution and instabilityin Figure 5. At openings greater than 30%, streamlines remain relatively uniform and stable. However, when the opening decreases below 20%, pronounced local vortices appear within the valve cavity, accompanied by recirculation and reattachment bubbles in the outlet pipe. These features indicate increased flow unsteadiness and turbulence intensity at small openings.

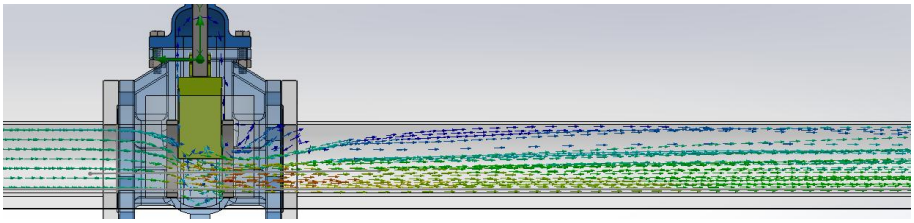
When the opening decreases to approximately 40% and further below 20%, recirculation regions expand significantly and eventually dominate the downstream flow field. This behavior not only reduces flow capacity but also increases the risk of erosion and particle deposition. Therefore, valve design must account for flow instability to mitigate excessive disturbances and erosion risks.



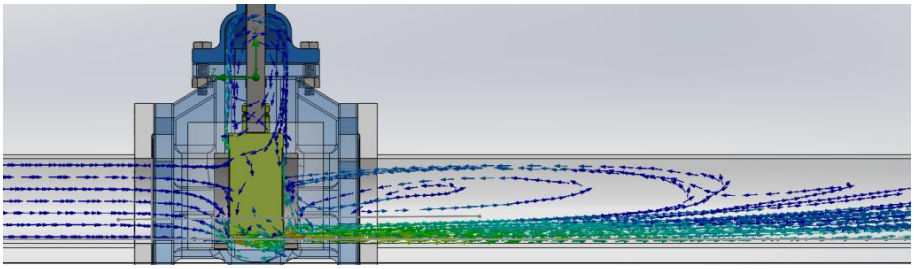
(a) 20% closed



(b) 40% closed



(c) 50% closed



(d) 90% closed

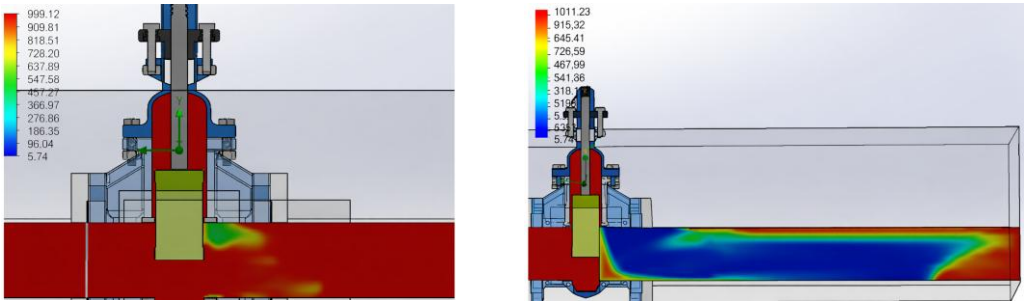
Figure 5. Streamline cross-section of the flow field

ISSN: 2472-3703 DOI: 10.6911/WSRJ.202602_12(2).0005

3.4. Cavitation Sensitivity

Cavitation analysis indicates that, as the valve opening decreases, the fluid density inside the valve undergoes significant variations. In particular, at valve openings of 50% and 90%, the local fluid density decreases from approximately 1000 kg/m^3 to about 450 kg/m^3, leading to pronounced negative-pressure regions and high-shear flow phenomena. The density contour plots shown in Figure 6 clearly illustrate this behavior. The regions of reduced density are mainly concentrated on the leeward side of the gate plate and within the near-wall boundary layer of the outlet pipe, suggesting that these areas are prone to cavitation initiation.

As the valve opening is further reduced, the cavitation region gradually expands. When the opening falls below 50%, the enlargement of the cavitation zone becomes particularly evident, with a marked intensification near the outlet section. Moreover, reducing the inlet flow velocity is shown to be an effective means of limiting the expansion of cavitation regions and mitigating the associated risks. These results indicate that valve design should place particular emphasis on minimizing cavitation-prone areas, especially under low-opening operating conditions. Suppression of cavitation not only improves the service life of the valve but also reduces erosion damage to the downstream piping system.



(a) 50% closed: density contour plot (b) 90% closed: density contour plot

Figure 6. Fluid cavitation mechanism based on density variation

4. CONCLUSION

Based on CFD and flow characteristic analysis of a DN100 industrial gate valve, the following conclusions are drawn:

(1) Pressure drop and pressure gradients increase significantly with decreasing opening. At an inlet velocity of 10 m/s, the total pressure drop increases continuously as the opening decreases from fully open to approximately 30%. The axial pressure distribution transitions from nearly uniform to highly non-uniform, with throttling losses becoming the dominant energy dissipation mechanism at small openings.

(2) Pronounced high-velocity jets and large-scale recirculation zones form at small openings. When the opening exceeds approximately 30%, flow remains relatively smooth and stable. As the opening decreases to around 40% and further below 20%, recirculation and reattachment bubbles increase markedly in the valve cavity and outlet pipe. The coexistence of high-speed jets and large vortical structures significantly enhances flow instability and turbulence intensity, reducing effective flow capacity and increasing erosion and deposition risks.

(3) Cavitation sensitivity increases significantly at medium and small openings. Under typical throttling conditions of 50% and 90% closure, local fluid density on the leeward side of the gate plate and near the outlet wall decreases sharply, forming cavitation-sensitive zones. When the opening falls below approximately 50%, cavitation regions expand considerably and concentrate near the outlet. Appropriate reduction of inlet velocity or optimization of throttling

ISSN: 2472-3703 DOI: 10.6911/WSRJ.202602_12(2).0005

geometry can effectively mitigate cavitation intensity and alleviate erosion and noise issues in industrial applications.

ACKNOWLEDGEMENTS

Supported by the Basic Research Fund of Provincial Universities in Heilongjiang Province (No. 145309638)

REFERENCES

[1] Jin, X. Design and flow field characteristics analysis of an ultra-supercritical safety valve [D]. Harbin University of Science and Technology, Harbin, China, 2024. DOI: 10.27063/d.cnki.ghlgu.2024.000388.

[2] Yan, X., Xu, J., Li, Z. G., Yu, G. B., & Jia, J. B. Numerical simulation and analysis of the opening and closing dynamic process of a spring-loaded safety valve [J]. Journal of Harbin University of Science and Technology, 2024, 29(1): 25–34. DOI: 10.15938/j.jhust.2024.01.003.

[3] Fu, B., Jing, P. Y., & Xia, W. Fluid dynamic analysis of regulating and energy-dissipating valves in long-distance water conveyance tunnels [J]. Water Resources Construction and Management, 2023, 43(5): 6–14. DOI: 10.16616/j.cnki.11-4446/TV.2023.05.02.

[4] Shi, L. X., Han, J., & Huang, Z. Q. Flow field analysis of a cryogenic butterfly valve based on CFX [J]. Equipment Manufacturing Technology, 2022(7): 29–33.

[5] Li, J., Lan, G., Li, X. Y., & Zhang, W. J. Water hammer analysis and protection of a million-kilowatt ISC indirect air-cooling unit circulating water system [J]. Electric Power Survey & Design, 2021(11): 24–27, 75. DOI: 10.13500/j.dlkcsj.issn1671-9913.2021.11.005.

[6] Mu, Y., Sun, B. J., & Zhang, F. CFD-based fluid analysis and structural optimization design of a check valve [J]. Valve, 2021(4): 183–186. DOI: 10.16630/j.cnki.1002-5855.2021.04.002.

[7] Qi, C. X. Analysis and optimization of the opening and closing process of a check valve considering fluid–structure interaction [D]. Lanzhou University of Technology, Lanzhou, China, 2021. DOI: 10.27206/d.cnki.ggsgu.2021.000626.